FACTA UNIVERSITATIS (NIŠ)
SER.: ELEC. ENERG. vol. 19, no. 1, April 2006, 147-156

Characteristics of Inductive Loops Applied in Thelematics

Bratislav Mirić, Darko Vučković, and Petar Spalević

Abstract: The intention of this paper is to give a bright review of a process triggering equipment that is connected to the inductive loop when a vehicle is moving above it.

First, we tried to approximate the bottom of the vehicle with rectangular loop. On that base we developed a simulation model of a vehicle moving above the loop.

Then we measured the triggering point on the real condition. The intention of these measurements was to find how the triggering point depends on position of the vehicle (vehicle offset) above the loop and how it depends on the vehicle velocity.

On the basis of the obtained results that are shown in this paper, it becomes more clear when the triggering of the equipment that is connected to the inductive loop occurs when a vehicle is moving above the loop.

Keywords: Thelematics, inductive loops, inductive coefficient.

1 Introduction

Inductive loops have been applied as sensors in thelematics (traffic flow management) for some time[1, 2]. These loops are also used as sensors in coordinated guiding of semaphores on magistral lines of communications (”green wave”), in control systems for traffic supervision (passing through the red light) and in detectors for presence in the parking lots and road toll payment stations.

In the last few years the traffic progression caused the development of the systems for traffic flow management, to provide better utilization of the roads. The applied solutions are to a great extent based on the tools and measures supported by computers. In that case computer takes on the guiding of the actual traffic situations in real time. The tools of traffic management are, in that sense, velocity regulation,

Manuscript received September 4, 2005.

The authors are with Faculty of Technical Science, Unuversity of Pristina, 38200 K. Mitrovica, Kneza Miloša 7, Serbia (e-mails: [bmiric, petarspalevic]@ftnkm.info).

traffic guiding and management by variable traffic signs whose messages are remote controlled, or other appropriate means by which unfavorable traffic situations could be overcome [3].

The generation of impulse in an inductive loop is based on the influence of conductive parts of the bottom of the vehicle on the inductive loop. The inductive loop is induced by a generator that works on the frequencies from 20 kHz to 200 kHz. Physical description of the impulse generation can be easily derived if proceeded from the assumption that metal parts of the bottom of vehicle can be described as an equivalent conductive surface, or simply an rectangular loop [4, 5, 6].

When a vehicle comes to the influential distance from inductive loop, so that generally exert influence on it, the coupling coefficient takes a small, but measurable value. As the vehicle reaches the inductive loop, it provides more influence on the loop, because the coupling coefficient increases.

When partial parts of the bottom of vehicle are maximally overlapped with the surface of inductive loop, the coupling coefficient takes maximal value. As the vehicle passes and moves away from inductive loop, it reduces its influence on the loop because the coupling coefficient reduces.

2 Induction Coefficient Between Two Rectangular Loops with Different Dimensions

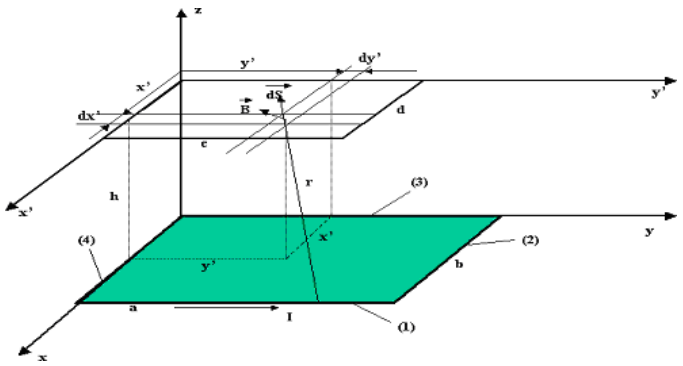

Fig. 1. Position of the two loops.

This is a general case of position of two loops in Decart coordinate system.

The metric normalized entire flux from edges of the rectangular (dimensions $a \times b$) loop through upper rectangular area (dimensions $c \times d$) is

$$\Phi_e = \Phi_1 + \Phi_2 + \Phi_3 + \Phi_4, \tag{1}$$

where we can see that the first component is determined as

$$\begin{aligned}\Phi_1 = {} & f_{11} + f_{12} - \frac{c_2}{2}\ln\frac{f_{12}-c_2}{f_{12}+c_2} + \frac{c_2}{2}\ln\frac{f_{11}-c_2}{f_{11}+c_2} \\ & - f_{13} + f_{14} - \frac{c_1}{2}\ln\frac{f_{13}-c_1}{f_{13}+c_1} + \frac{c_1}{2}\ln\frac{f_{14}-c_1}{f_{14}+c_2} \\ & + f_{15} - f_{16} + \frac{a-c_2}{2}\ln\frac{f_{15}-(a-c_2)}{f_{15}+(a-c_2)} - \frac{a-c_2}{2}\ln\frac{f_{16}-(a-c_2)}{f_{16}+(a-c_2)} \\ & - f_{17} + f_{18} - \frac{a-c_1}{2}\ln\frac{f_{17}-(a-c_1)}{f_{15}+(a-c_1)} - \frac{a-c_1}{2}\ln\frac{f_{18}-(a-c_1)}{f_{18}+(a-c_1)}\end{aligned} \tag{2}$$

and

$$\begin{aligned} f_{11} &= \sqrt{c_2^2+(b-d_1)^2+h^2} & f_{11} &= \sqrt{c_2^2+(b-d_2)^2+h^2} \\ f_{13} &= \sqrt{c_1^2+(b-d_1)^2+h^2} & f_{13} &= \sqrt{c_1^2+(b-d_2)^2+h^2} \\ f_{15} &= \sqrt{(a-c_2)^2+(b-d_2)^2+h^2} & f_{15} &= \sqrt{(a-c_2)^2+(b-d_1)^2+h^2} \\ f_{17} &= \sqrt{(a-c_1)^2+(b-d_2)^2+h^2} & f_{17} &= \sqrt{(a-c_1)^2+(b-d_1)^2+h^2} \end{aligned} \tag{3}$$

Also, the second term of this normalized entire flux is

$$\begin{aligned}\Phi_2 = {} & f_{21} - f_{22} - \frac{d_2}{2}\ln\frac{f_{22}-d_2}{f_{22}+d_2} + \frac{d_2}{2}\ln\frac{f_{21}-d_2}{f_{21}+d_2} \\ & - f_{23} + f_{24} - \frac{d_1}{2}\ln\frac{f_{23}-d_1}{f_{23}+d_1} + \frac{d_1}{2}\ln\frac{f_{24}-d_1}{f_{24}+d_2} \\ & + f_{25} - f_{26} + \frac{b-d_2}{2}\ln\frac{f_{25}-(b-d_2)}{f_{25}+(b-d_2)} - \frac{b-d_2}{2}\ln\frac{f_{26}-(b-d_2)}{f_{26}+(b-d_2)} \\ & + f_{27} - f_{28} - \frac{b-d_1}{2}\ln\frac{f_{28}-(b-d_1)}{f_{28}+(b-d_1)} + \frac{b-d_1}{2}\ln\frac{f_{27}-(b-d_1)}{f_{27}+(b-d_1)}\end{aligned} \tag{4}$$

where

$$\begin{aligned} f_{11} &= \sqrt{(a-c_1)^2+d_2^2+h^2} & f_{11} &= \sqrt{(a-c_2)^2+d_2^2+h^2} \\ f_{13} &= \sqrt{(a-c_1)^2+d_1^2+h^2} & f_{13} &= \sqrt{(a-c_1)^2+d_1^2+h^2} \\ f_{15} &= \sqrt{(a-c_2)^2+(b-d_2)^2+h^2} & f_{15} &= \sqrt{(a-c_1)^2+(b-d_2)^2+h^2} \\ f_{17} &= \sqrt{(a-c_1)^2+(b-d_1)^2+h^2} & f_{17} &= \sqrt{(a-c_2)^2+(b-d_1)^2+h^2} \end{aligned} \tag{5}$$

We can represent the third term with following equation

$$\begin{aligned}\Phi_3 = {} & f_{31} - f_{32} - \frac{a-c_2}{2}\ln\frac{f_{31}-(a-c_2)}{f_{31}+(a-c_2)} + \frac{a-c_2}{2}\ln\frac{f_{32}-(a-c_2)}{f_{32}+(a+c_2)} \\ & + f_{33} + f_{34} - \frac{a-c_1}{2}\ln\frac{f_{34}-(a-c_1)}{f_{34}+(a-c_1)} + \frac{a-c_1}{2}\ln\frac{f_{33}-(a-c_1)}{f_{33}+(a-c_1)} \\ & + f_{35} - f_{36} - \frac{c_2}{2}\ln\frac{f_{36}-c_2}{f_{36}+c_2} + \frac{c_2}{2}\ln\frac{f_{35}-c_2}{f_{35}+c_2} \\ & - f_{37} + f_{38} - \frac{c_1}{2}\ln\frac{f_{37}-c_1}{f_{37}+c_1} - \frac{c_1}{2}\ln\frac{f_{38}-c_1}{f_{38}+c_1}\end{aligned} \tag{6}$$

where

$$\begin{aligned} f_{11} &= \sqrt{(a-c_2)^2+d_1^2+h^2} & f_{11} &= \sqrt{(a-c_2)^2+d_2^2+h^2} \\ f_{13} &= \sqrt{(a-c_1)^2+d_1^2+h^2} & f_{13} &= \sqrt{(a-c_1)^2+d_1^2+h^2} \\ f_{15} &= \sqrt{c_2^2+d_2^2+h^2} & f_{15} &= \sqrt{c_2^2+d_1^2+h^2} \\ f_{17} &= \sqrt{c_1^2+d_2^2+h^2} & f_{17} &= \sqrt{c_1^2+d_1^2+h^2} \end{aligned} \tag{7}$$

At the end, the last component of the normalized entire flux is

$$\begin{aligned}\Phi_4 = {} & f_{41} - f_{42} - \frac{b-d_2}{2}\ln\frac{f_{41}-(b-d_2)}{f_{41}+(b-d_2)} + \frac{b-d_2}{2}\ln\frac{f_{42}+(b-d_2)}{f_{42}+(b+d_2)} \\ & + f_{43} - f_{44} - \frac{b-d_1}{2}\ln\frac{f_{44}-(b-d_1)}{f_{44}+(b-d_1)} + \frac{b-d_1}{2}\ln\frac{f_{43}-(b-d_1)}{f_{43}+(b-d_1)} \\ & + f_{45} - f_{46} - \frac{d_2}{2}\ln\frac{f_{46}-d_2}{f_{46}+d_2} + \frac{d_2}{2}\ln\frac{f_{45}-d_2}{f_{45}+d_2} \\ & - f_{47} + f_{48} - \frac{d_1}{2}\ln\frac{f_{47}-d_1}{f_{34}+d_1} - \frac{d_1}{2}\ln\frac{f_{48}-d_1}{f_{48}+d_1}\end{aligned} \tag{8}$$

where

$$\begin{aligned} f_{11} &= \sqrt{(b-d_2)^2+c_1^2+h^2} & f_{11} &= \sqrt{(b-d_2)^2+c_2^2+h^2} \\ f_{13} &= \sqrt{(b-d_1)^2+c_2^2+h^2} & f_{13} &= \sqrt{(b-d_1)^2+c_1^2+h^2} \\ f_{15} &= \sqrt{d_2^2+c_2^2+h^2} & f_{15} &= \sqrt{d_2^2+c_1^2+h^2} \\ f_{17} &= \sqrt{d_1^2+c_2^2+h^2} & f_{17} &= \sqrt{d_1^2+c_1^2+h^2} \end{aligned} \tag{9}$$

The normalized cross-induction coefficient between two rectangular loops is

$$M = \frac{\Phi_e}{I} \tag{10}$$

We shall now consider the case shown on Fig. 2. One loop (in first - approximation bottom of vehicle) is moving above the second induction loop. The position of the vehicle is determined by vehicle offset Δx. Dimensions of vehicle are 4.7 $\times$ 1.6 m and dimensions of the induction loop are 1.5 $\times$ 1.5 m.

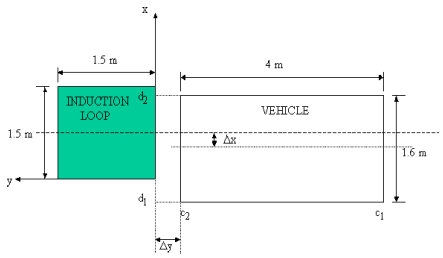

Fig. 2. Dimensions of the vehicle.

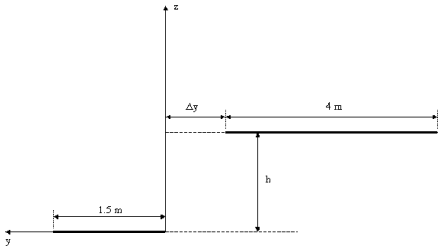

Fig. 3. Distance between the bottom of the vehicle and loop is *h*.

The vertical distance between loop (Fig.3) is h. Two extreme cases are when Δx=1650 mm or $\Delta x = -1650$ mm.

Next figures are show the induction coefficient M in function of vehicle offset Δx and the position of vehicle above induction loop Δy, for different vertical distance two loops.

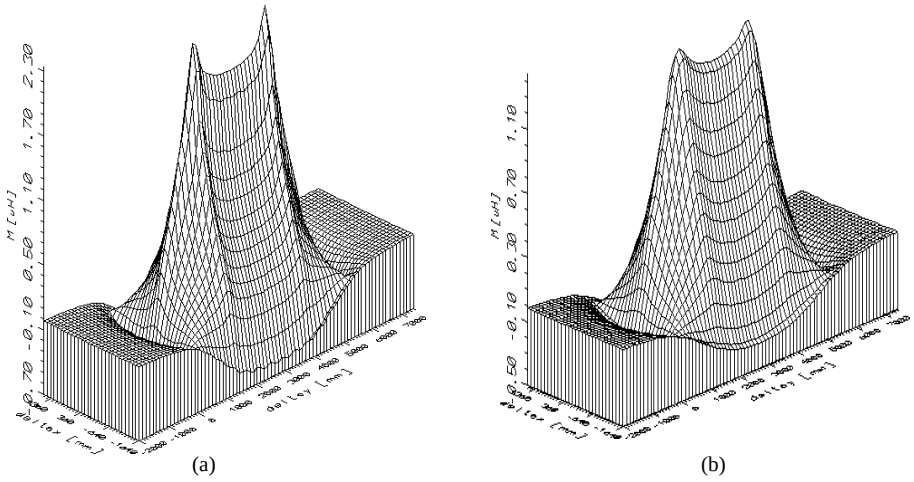

(a) (b)

Fig. 4. Induction coefficient M in function of vehicle offset Δx and position of vehicle above induction loop δy, for different vertical distance two loops.

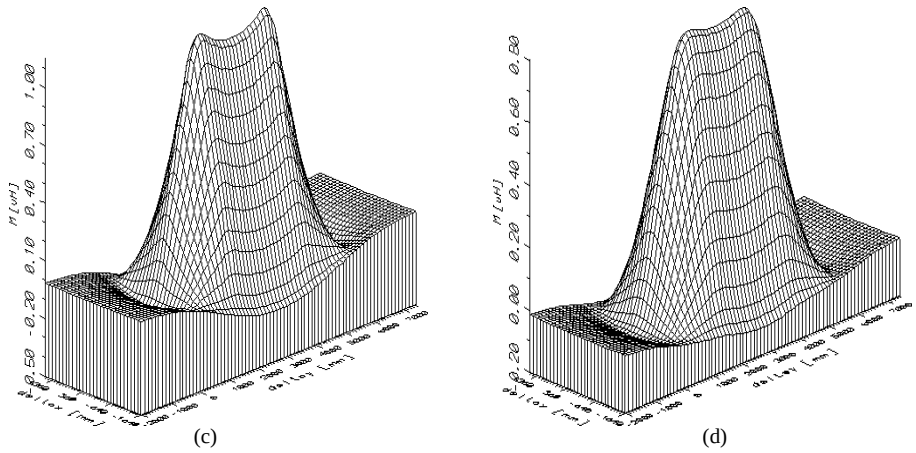

(c) (d)

Fig. 4. (cont'd) (a) Induction coefficient M in function of the vehicle offset (Δx) and position of the vehicle above induction loop (Δy) loop (Δx) for $h = 5$ cm. (b) Induction coefficient M in vehicle offset (Δx) and position position of the vehicle above induction loop (δy) for $h = 20$ cm. (c) Induction coefficient M in function of vehicle offset (Δx) and position of the vehicle above induction loop (Δy) for $h = 30$ cm (d) Induction coefficient M in function of vehicle offset (Δx) and position of the vehicle above induction loop (Δy) for $h = 50$ cm.

3 Experimental Results

The induction loop was placed on the road inside Physikalisch Techniche Bundesanstalt-PTB near Bessel bau Fig.5,6 and 7. The figures show the position of induction loop, used equipment and marks on the road.

Fig. 5. Induction loop and measuring disposition

Dimensions of the loop and its connection to the measuring equipment that was placed in PTB laboratory are shown in Fig.8

This measurement was performed under the known conditions (type of vehicle,

Fig. 6. Induction loop with marks on the road.

position against the loop) [7, 8, 9, 10]. The vehicle was OPEL Omega-A and it passed-through over the loops 46 times with different velocities and path but without acceleration. With this second measurement (with video camera) we tried to locate the moment (position of vehicle above the loop) when camera is triggered by equipment TRAFFIPHOT III fabricated by Traffipax-Vetrieb from Düsseldorf. For this purpose we took corresponding frame from the digitized video camera signal (video camera near Camera A on Fig.8).

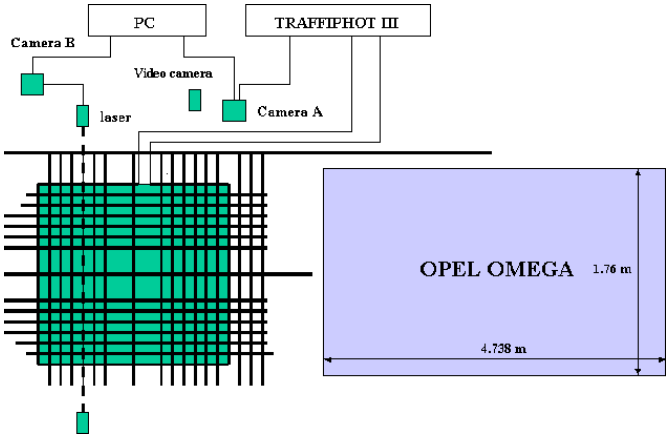

Fig. 7. Sketch of the measuring disposition.

Camera A was triggered by TRAFFIPHOT III that was connected to the induction loop. Camera B was triggered when front part of vehicle cut the laser beam. Laser beam was 1.11 m from the beginning of the loop. The beam was about 70

cm above the road. Vehicle cut laser beam with its front part where OPEL mark is located.

The time delay of digital camera is 40 ms but also we must take into account the time delay of TRAFFIPHOT equipment. So, whole time delay from the moment when vehicle triggered the TRAFFIPHOT to the moment when camera get a photo is greater than 40 ms. Position of vehicle on the photo is not the position of vehicle when triggering occurs. For different velocities real position of vehicle in that moment differs from the position on photo. The triggering take place $\Delta S = v\Delta t$ before vehicle position on photo. For $\Delta t = 40$ ms and vehicle velocity 50 km/h ΔS is 55.5 cm.

Next figures shown a few photos from Camera A. Original digital photo has two half pictures and we separated them with Adobe Photoshop program. Vehicle velocity was measured by laser equipment. In all these photos vehicle velocity was about 30 km/h but vehicle offset Δx was different. With y_t we marked y coordinate of front vehicle part when the photo was taken.

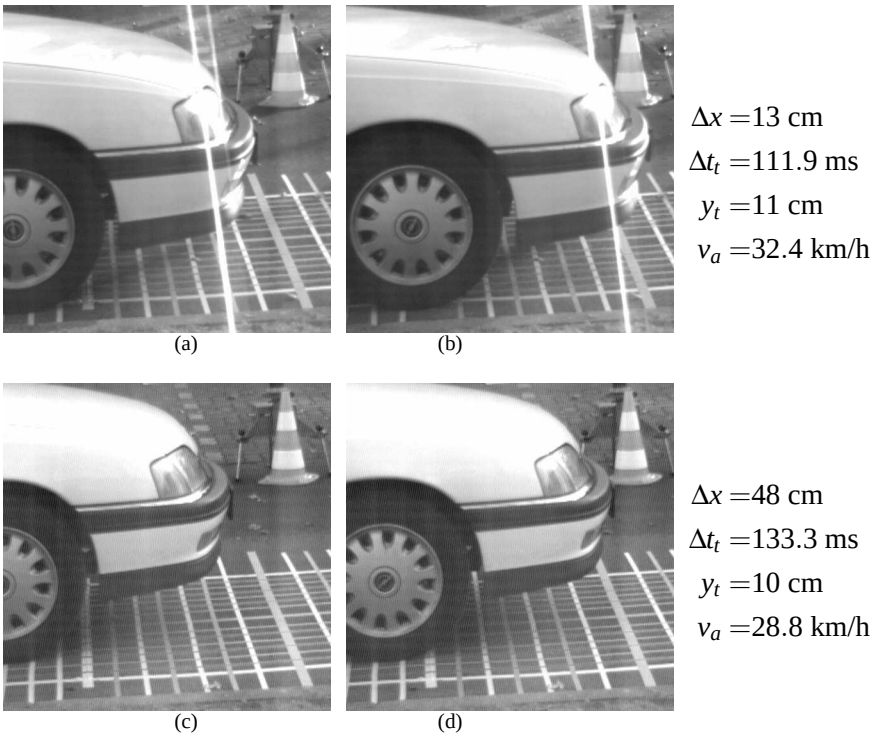

Fig. 8. Photos from camera A. Left photo is first half part picture and right photo is second half picture.

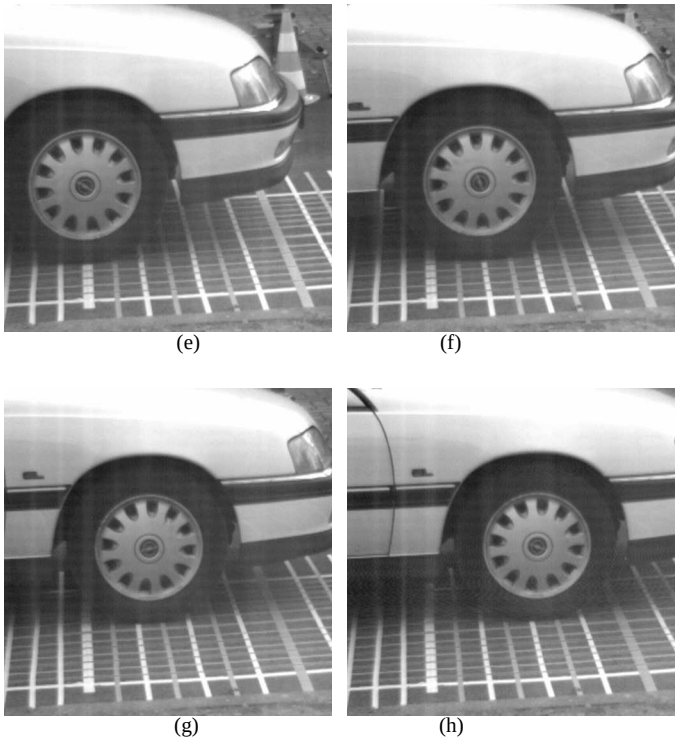

Δx =65 cm
Δt_t =83.5 ms
y_t =33 cm
v_a =234 km/h

Δx =100 cm
Δt_t =58 ms
y_t =59 cm
v_a =32.4 km/h

Fig. 8. (cont'd) Photos from camera A. Left photo is first half part picture and right photo is second half picture.

At the end of the loop, the front part of vehicle cut the laser beam (Fig.8). The difference between the moment when vehicle cut laser beam t_1 and the moment when vehicle triggered TRAFFIPHOT equipment t_2 is very precisely measured and

$$\Delta t = t_2 - t_1, \tag{11}$$

with v_a [km/h] we marked approximate value of vehicle velocity calculated from the photo.

4 Conclusion

On the basis of conducted measurements and obtained atlas of photographs [1], it can be concluded that the triggering point of the device connected to the inductive loop depends on the distance between the bottom of the vehicle and the inductive loop. It means that triggering of device connected to the inductive loop will occur

later in the case of long vehicle (LKV) than in the case of automobile (PKV). For motorcycle no triggering was registrated during its passage above inductive loop, due to its small surface and negligible value of induction coefficient between the bottom of the motorcycle and inductive loop.

Triggering point of the vehicle depends also on the vehicle offset between vehicle and loop axes, in other words on the effective surface covering the inductive loop.

Our measurements indicate that the vehicle distance on which the induction coefficient reaches its critical value when triggering of device occurs, depends above all on the vehicle offset. The vehicle velocity does not influence significantly the triggering point of connected device.

References

[1] B. Miricć, "Inductive loops, theory and measurements," Physikalisch-Technische Bundesanstalt," PTB Bericht, Laboratorium 1.63, Dec. 1997.

[2] A. Marković, J. Kapković, C.-H. Luehrs, M. Michel, B.Mirić, and F. Jaeger, "Geschwindigkeitsmessungen im strassenverkehr," Physikalisch-Technische Bundesanstalt, Expert Verlag Stuttgart, SRN, Tech. Rep., 1996.

[3] A. Marković and B. Mirić, "Untersuchungen zur verwendung von induktionsschleifen als sensoren von geschwindigkeitsmessgeraeten," Physikalisch-Technische Bundesanstalt, PTB Bericht, Laboratorium 1.63 PTB-1.1.63-95-1, 1995.

[4] H. Goydke, F. Jäger, M. Michel, A. Marković, and A. Mirić, "Pruefverfahren für geschwindigkeitsmessagerate," Braunschweig, pp. 160–161, Dec. 1992.

[5] B. Mirić and A. Marković, "Loop phase detector, part one," Physikalisch-Technische Bundesanstalt, PTB Laborbericht PTB-1.63-95-1, Sept. 1992.

[6] ——, "Loop phase detector, part two," Physikalisch-Technische Bundesanstalt, PTB Laborbericht PTB-1.63-92-1, Dec. 1992.

[7] Jäger, F. Meende, and R. Michel, "77 ghz traffic radar sensor for speed enforcement measuring speed and distance," in *Veröffentlichungen zum 7th Weltkongress über Intelligente Transportsysteme (ITS)*, Turin (Italien), Nov. 8, 2000.

[8] F. Jäger (Herausgeber), "Eichung von stationären geschwindigkeitsmessanlagen/-rotlichtüberwachungsanlagen," Physikalisch-Technische Bundesanstalt, Braunschweig, PTB-Bericht PTB-1.21-2003-1, Mar. 2003.

[9] F. Mhrtens and F. Jäger, "Die prüfung von fahrtschreibern der neueren bauart krafthand," *Technisches Fachmagazin für das Kraftfahrzeughandwerk*, no. 9, pp. 58 – 64, 2003, iSSN 0023-4435.

[10] F. Jäger, U. Grottker, H. Schrepf, and W. Guse, "Prediction signal processing for speed enforcement measuring speed and distance," *Computer Standards & Interfaces*, vol. 28, pp. 327–335, 2006.